

# Detection of Neutrons

R. Nolte

*Physikalisch-Technische Bundesanstalt, Bundesallee 100, 38116 Braunschweig, Germany*

## Table of contents

- 1 Introduction**
  - 1.1 Neutrons in Science and Technology
  - 1.2 Interaction of Neutrons with Matter
- 2 Neutron detection**
  - 2.1 Detectors for thermal and slow neutrons
  - 2.2 Detectors for fast neutrons
    - 2.2.1 Moderating detectors
    - 2.2.2 Recoil detectors
      - 2.2.2.1 General aspects
      - 2.2.2.2 Proportional counters
      - 2.2.2.3 Scintillation detectors
      - 2.2.2.4 Recoil telescopes
    - 2.2.3 Fission ionization chambers
  - 2.3 Techniques for neutron measurements
    - 2.3.1 Time-of-flight measurements
    - 2.3.2 Neutron spectrometry
      - 2.3.2.1 General aspects
      - 2.3.2.2 High-resolution spectrometry
      - 2.3.2.3 Low-resolution spectrometry
    - 2.3.3 Spatial neutron distributions
- 3 Absolute methods, quality assurance**
  - 3.1 Associated particle methods
  - 3.2 International key comparisons

## Abstract

These notes summarize two lectures on the detection of fast and slow neutrons. The focus is on the basic detection techniques and detector principles, i.e. detectors based on the moderation of fast neutrons and on the detection of recoil particles. The most important techniques for the measurements of the energy distribution of neutron, namely time-of-flight and pulse-height spectrometry are presented. Finally a short overview over the measurement of spatial neutron distributions and on methods for quality assurance of neutron measurements is given.

## 1. Introduction

### 1.1 Neutrons in Science and Technology

In 1932, Sir James Chadwick repeated and correctly explained [CHA32] earlier experiments of the Curie's by postulating an instable neutral particle which together with the protons constitutes the atomic nucleus. These experiments already showed all relevant features of a modern neutron detector. Neutrons were produced by a nuclear reaction and detected by conversion to a charged particle in a 'radiator'. Fig. 1 shows a sketch of Chadwick's experiment and a photograph of his apparatus.

Techniques for the detection of neutrons are required in many fields of physics and technology. First of all, the neutron is a unique laboratory for studying the fundamental properties of matter. For example, experiments searching for a permanent electrical dipole moment contain a detector for polarized ultra cold neutrons. In solid state physics the magnetic dipole moment of the neutron can be used to study the magnetic structure of solids by neutron scattering. In nuclear physics, the detection of neutrons yields important information about the dynamics of nuclear reaction.

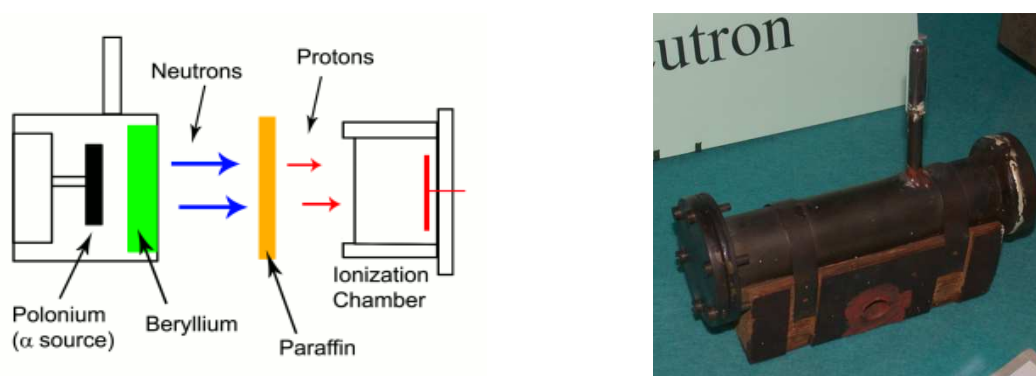


**Fig. 1:** Sketch of the Chadwick's experiment which led to the discovery of the neutron (left). The photograph shows Chadwick's apparatus (right).

The most important use of neutrons, however, is still the production of energy in fission reactors, and eventually also in future fusion reactors. Here neutron measurements are vital for the control of the reactors. Even in space science and astrophysics neutron detection plays a role. The measurement of neutron capture cross sections is important to improve the understanding of the synthesis of the elements in eruptive stellar processes. Despite their finite mean lifetime of about 880 s, a fraction of the neutrons produced in the sun can reach neutron monitors installed at high altitude on earth. Hence, these neutrons can be used to diagnose eruptive processes on the solar surface.

### 1.2 Interaction of Neutrons with Matter

Since neutrons are uncharged, they can only be detected by registering the charged particles or photons emitted in neutron-induced nuclear reactions, e.g. recoil nuclei from elastic or inelastic scattering  ${}^A\text{X}(n,n){}^A\text{X}$  and  ${}^A\text{X}(n,n'\gamma){}^A\text{X}$ , photons from radiative capture  ${}^A\text{X}(n,\gamma){}^{A+1}\text{X}$ , radioactive nuclei produced in  ${}^A\text{X}(n,2n){}^{A-1}\text{Y}$  reactions or fission fragments from neutron-induced fission. For thermal, epithermal and slow neutrons with energies below 10 keV, reactions with large positive  $Q$ -values are required to produce secondary charged particles of sufficient energy for easy detection. Because of the high  $Q$ -value, the energy of the secondary particles is almost independent of the small energy of the neutron. Hence, detectors for low-energy neutrons are used as pure neutron counters in most cases.

In contrast, detectors for fast neutrons are generally used as neutron spectrometers, i.e. the energy of the secondary particle depends significantly on the neutron energy and inversion

procedures can be applied to infer the neutron energy. The most important example is elastic scattering  ${}^A\text{X}(n,n){}^A\text{X}$ . The energy  $E_{\text{rec}}$  of the recoil nucleus is related to the energy  $E_n$  of the incident neutron by

$$E_{\text{rec}} = E_n \frac{4A}{(A+1)} \cos^2(\phi_{\text{rec}}^{\text{lab}}) \quad (1)$$

where  $\phi_{\text{rec}}^{\text{lab}}$  denotes the emission angle of the recoil nucleus in the laboratory system. Moreover, the energy distribution ( $dN/dE_{\text{rec}}$ ) of the recoil nuclei has the same shape as the differential scattering cross section ( $d\sigma/d\Omega^{\text{cm}}$ ) in the center-of-mass system,

$$\frac{dN}{dE_{\text{rec}}} \propto \frac{1}{E_n} \frac{(A+1)^2}{4A} \left( \frac{d\sigma}{d\Omega^{\text{cm}}} \right) (E_n). \quad (2)$$

In the fast energy range nuclear reactions with high and smoothly varying cross sections are best suited for the detection of neutrons. The list of suitable reactions is almost identical with the collection of neutron cross section standards shown in Fig. 2, plus some dosimetry standards, e.g.  ${}^{209}\text{Bi}(n,f)$  for high energy neutrons, and a few additional reactions such as  ${}^{155,157}\text{Gd}(n_{\text{th}},\gamma)$ .

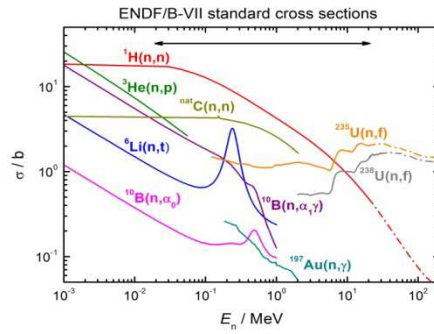


**Fig. 2:** Neutron cross section standards.

The detection of neutron is covered in several monographs on neutron physics [MAR60], [BEC64] or in textbooks on nuclear measurement techniques [KNO10], [LEO09]. Moreover, the proceedings of the regular conferences on Nuclear Data in Science and Technology, the SORMA and Crete conferences as well as those of more specialized workshops provide additional and more up to date material. Useful material can also be found in a special volume on neutron metrology published in Metrologia [THO11].

## 2. Neutron Detection

### 2.1 Detectors for Slow Neutrons

Due to the low energy of thermal neutrons, only reactions with high  $Q$ -values can be employed to detect them. In addition, inherent signal amplification inside the detector is an advantage. This is why proportional counters with the counting gases  ${}^3\text{He}$  and  ${}^{10}\text{BF}_3$  are used frequently. The cross sections  $\sigma$  of the  ${}^3\text{He}(n,p)\text{T}$  ( $Q = 0.764$  MeV),  ${}^{10}\text{B}(n,\alpha_0){}^7\text{Li}$  ( $Q = 2.792$  MeV) and  ${}^{10}\text{B}(n,\alpha_1\gamma){}^7\text{Li}$  ( $Q = 2.310$  MeV) reactions are inversely proportional to the neutron velocity  $v$  up to an energy of about 10 keV. The reaction rate

$$\frac{dN}{dt} = \int \frac{\sigma_0 v_0}{v} n_E v dE = \sigma_0 v_0 n \quad (3)$$

is independent of the energy distribution and the detector can be used to measure the total density  $n$  of slow neutrons. Here  $\sigma_0$  is the so-called Westcott cross section, i.e. the cross section  $\sigma(v_0)$  at a velocity  $v_0$  of 2200 m/s.

The total energy of the charged reaction products is determined by the  $Q$ -value of the reaction products. Hence, the pulse-height spectra of the counters are almost independent of the neutron energy. Due to the large range of the secondary particles they are strongly affected by wall effects, i.e. incomplete energy deposition in the counting gas. A pulse-height distribution of a  $^{10}\text{BF}_3$  proportional counter is shown in Fig. 3

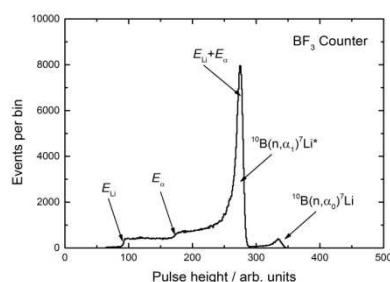


**Fig. 3:** Pulse-height distribution of a  $^{10}\text{BF}_3$  proportional counter. The structures resulting from incomplete energy deposition by alpha particles or  $^7\text{Li}$  ions are indicated.

The advantage of proportional counters is that they can be constructed in various sizes and geometrical shapes. The pressure of the counting gases can be varied as well. Hence, the sensitivity of the detector can be easily adapted to the measurement problem. The sensitivity has, however, usually to be determined by a calibration in a reference neutron field because the sensitive volume depends on the details of the electrical field and the pressure of the counting gas which are usually not known well enough. The counters are also sensitive to photons, but due to the large range of the secondary electrons in the counting gases, photon induced events can usually be discriminated easily using a pulse-height threshold.

Other useful detectors for thermal and slow neutrons are  $^{235}\text{U}$  fission ionization chambers and  $^6\text{LiI}$  scintillation detectors. These detectors use the  $^{235}\text{U}(n,f)$  reaction ( $Q \approx 200$  MeV) and  $^6\text{Li}(n,t)^4\text{He}$  ( $Q = 4.78$  MeV). Fig. 4 shows the cross sections for the most important reaction used for detection of slow neutrons.

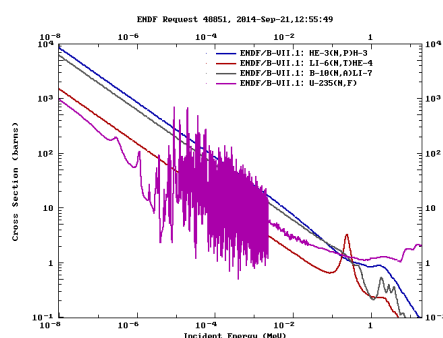


**Fig. 4:** Cross sections for the most important reaction used for the detection of slow neutrons.

## 2.2 Detectors for fast neutrons

### 2.2.1 Moderating detectors

In the energy range of fast neutrons cross section are much smaller than in the energy range for slow neutrons. Hence, it is attractive to construct a detectors for fast neutrons by covering a detector for thermal neutrons, e.g. a  $^3\text{He}$  or  $^{10}\text{BF}_3$  proportional counter, with a moderator which reduces the energy of the fast neutrons by multiple scattering off hydrogen so that they can be detected efficiently by the thermal detector. Due to the high detection cross

section and the large effective size of the moderator, such detectors have a high fluence response  $R_\Phi = N/\Phi$ , where  $N$  denotes the number of detected events and  $\Phi$  the fluence of incident neutrons.

The most important representative of this kind of neutron detectors is the long counter [HAN47]. It consists of a cylindrical polyethylene moderator which surrounds a  $^3\text{He}$  or  $^{10}\text{BF}_3$  proportional counter. The moderator is split into an outer annular part and an inner part which are separated by a cadmium layer. This design reduces the sensitivity to neutrons incident from the sides. The energy dependence of the fluence response at lower energies is increased by holes or grooves arranged in the front face close to the proportional counter. As shown in Fig. 5, this results at an almost flat response in the energy range between 10 keV and 10 MeV.

For neutron energies below 10 MeV, the moderation process is mainly determined by elastic scattering off hydrogen and carbon nuclei. The cross sections for these reactions are known with small uncertainties. The response of a long counter can therefore be calculated accurately using standard Monte Carlo simulation programs. The disadvantage of the long counter principle is the loss of all information on the neutron energy. Due to the large moderator time of several ten microseconds, long counters are also not suitable for time-of-flight measurements.

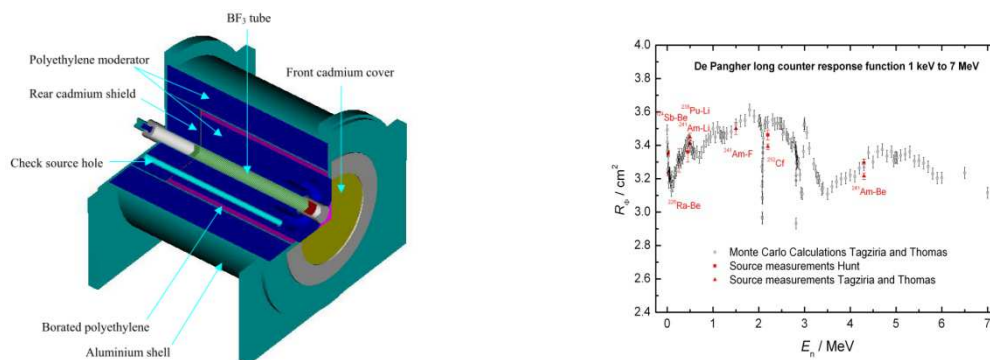


**Fig. 5:** Layout of a de Pangher long counter (left), energy dependence of the fluence response of this detector (right) [ROB04]. The preferred directions for the neutrons is parallel to the cylindrical axis from the right.

Moderator-type detectors are used to efficiently detect neutrons from neutron-producing reactions with small cross sections [GOM10]. The neutron source is usually placed in the center of the moderator and thermal detectors are located on concentric rings in the moderator. An interesting variant of the moderator-type detector for nanosecond-pulsed collimated neutron beams is the so-called ‘black detector’ [POE73]. Here, the moderator consists of a liquid scintillator. The collimated beam is guided to the detector center through a channel. The scintillation light is registered by several photomultipliers. Due to the strong quenching of the production of scintillation light by low-energy recoil protons, the timing of the photomultiplier signals is determined only by the first few scattering events. Hence, an almost flat detection efficiency of almost 90% can be combined with a time resolution of only a few nanoseconds.

## 2.2.2 Recoil detectors: prop. counters, scintillation detectors, recoil telescopes

### 2.2.2.1 General aspects

The most important type of detectors for fast neutrons are those which directly detect recoil particles, in particular recoil protons resulting from elastic neutron-proton (np) scattering. The recoil particles are either produced in the detector itself (target = detector) or in a separate radiator. In the latter case the recoil particles are detected in a detector or a

combination of stacked detectors (detector telescope) to reduce the influence of neutron-induced background. This methods allows the energy of the neutron to be measured together with the neutron fluence, i.e. the detector can be used as a spectrometer. For neutron energies below 20 MeV the relative uncertainties of the n-p scattering cross section  $\sigma_{np}$  is smaller than 0.5 %. The detection efficiency of these detector can often be calculated rather reliably because of the simple detection process and the well-known cross sections. The situation is somewhat different for the neutron energy range above 20 MeV. Here the differential np scattering cross section is only known to about 5% at backward angles [ARN91].

### 2.2.2.2 Proportional counters

At neutrons energies well below 1 MeV solid states radiators cannot be employed because of the increased energy loss of the recoil protons. Instead gaseous radiators have to be used. Gas amplification in proportional chambers facilitates the detection of recoil protons with energies of a few keV. As an exmaple, Fig. 6 shows a cylindrical proportional counter which is used as a reference instrument for neutron fluence measurements. Hydrogen/methane mixtures and propane are used as counting gases. The sensitive volume is defined by field tubes F and the cylindrical cathode C. The anode wire A has a diameter of 50  $\mu\text{m}$ . The counter is operated with hydrogen/methane mixtures or propane.

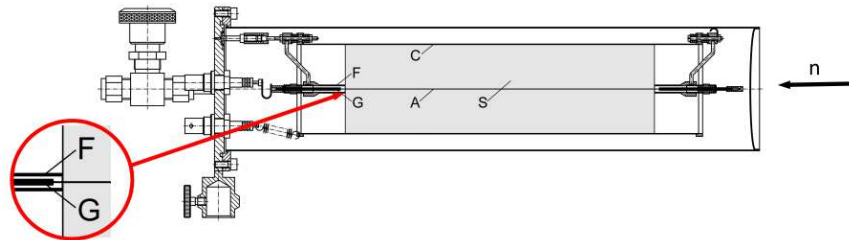


**Fig. 6:** Proportional counter for the measurement for the fluence of neutron with energies below about 1.5 MeV. The sensitive volume is shaded in grey. It is defined by the field tubes F and the cylindrical cathode C. The anode wire A has a diameter of 50  $\mu\text{m}$ . The counter is operated with hydrogen/methane mixtures or propane.

The shape of the pulse-height distribution measured with this detector should be rectangular because the differential np scattering cross section in the center-of-mass system is isotropic at energies below 5 MeV. However, as shown in Fig. 7, incomplete energy deposition by recoil protons escaping from the sensitive volume (wall effect) as well as the energy dependence of the energy  $W$  required to produce an ion pair modifies the expected rectangular shape.

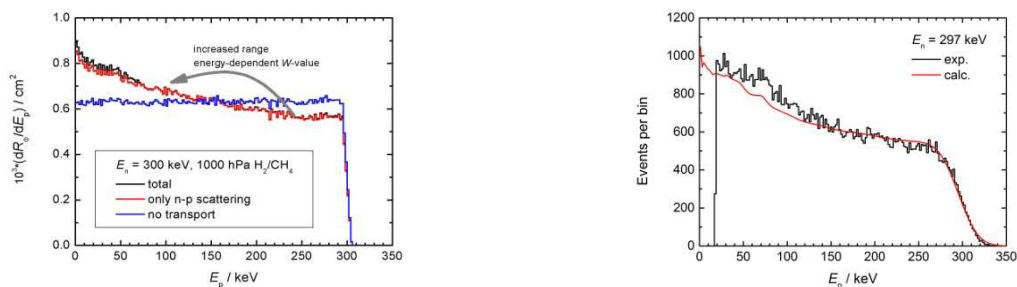


**Fig. 7:** The left panel shows a simulated pulse-height distribution for the proportional counter shown in Fig. 6. The neutron energy was 300 keV. The blue histogram is the ‘ideal’ response while the red and black histogram show the modifying effects of proton transport,  $W$ -value and carbon recoils. The right panel shows the experimental response to 297 keV neutrons (histogram) together with a Monte Carlo simulation (red line).

### 2.2.2.3 Scintillation detectors

At higher neutron energies, the target = detector principle is employed in organic scintillation detectors. Actually, this kind of detector is probably the most intensively used ‘working horse’ of neutron physics. Organic scintillation detectors are either organic crystals like anthracen or stilbene, or consist of an aromatic solvent in which one or more fluors are dissolved. The solvent can either be a liquid (liquid scintillator) or a polymer (plastic scintillator). The secondary electrons produced during the slowing-down of charged particles excite the delocalized  $\pi$  electrons in the benzene rings. The kinetics of population and de-population of the various excited states, in particular the competition between radiative and non-radiative de-excitation, determines the scintillation process [BRO79]. The scintillation light produced by the ionizing particles consists of a fast component with a decay time in the order of 10 ns (prompt fluorescence), and a slow non-exponential component with effective decay times in the order of a few hundred nanosecond (delayed fluorescence). Due to the combination of the different fluors the mean wavelength of the scintillation light is shifted from the near ultraviolet to the blue wavelength region where it can be effectively detected using photomultiplier (PMT) tubes.

The total amount of scintillation light depends on the ionization density of the charged particle. This causes the non-linear dependence of the amount of scintillation light on the energy of the charge particle. The so-called ‘quenching’ is dominant for protons and heavier particles with a strong variation of the differential energy loss ( $dE/dx$ ), but also observed for electrons with energies below a few keV. Moreover, also the relative contribution of the prompt and delayed components can depend on the ionization density. This facilitates the discrimination of electrons from heavier charged particles, e.g. recoil protons, or secondary alpha particles. Hence neutron-induced events can be discriminated from photon-induced background by analyzing the decay of the scintillation light. This technique is termed pulse-shape discrimination (PSD). Fig. 8 shows the schematic energy dependence of the integral scintillation light yield (light output function) and typical waveforms for the decay of the scintillation for organic scintillators.

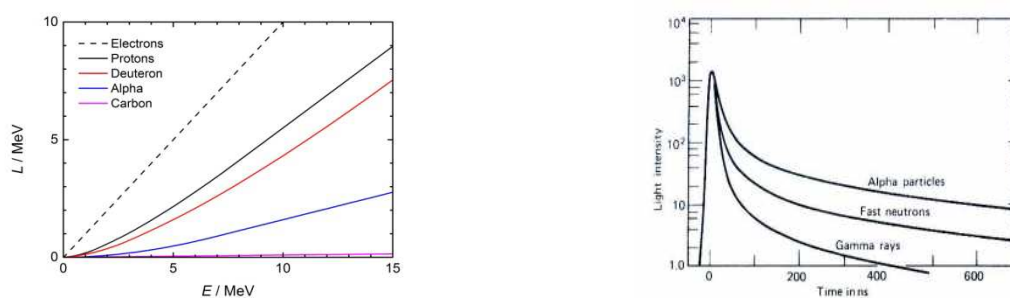


**Fig. 8:** The decay of the scintillation light observed for particles of different ionization density in organic scintillators is shown schematically on the right panel. The left panel shows the integral light yield normalized to that of high-energy electrons which depends almost linearly on the electron energy.

Fig. 9 shows how different particle species can be separated in a two dimensional distribution of events sorted according the integral light yield (horizontal axis) and a second parameter related to the effective decay time of the signal (vertical axis).

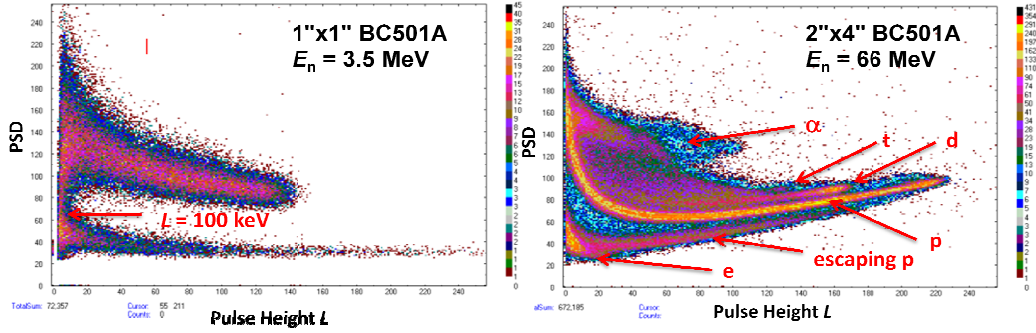


**Fig. 8:** Separation of different particle species of secondary particles in a liquid scintillation detector.

In the past, the PSD capability was only observed for liquid scintillators, but recently PSD was also demonstrated for solid organic scintillators where the secondary fluors are dissolved in a plastic matrix [ZAI12]. Table 1 summarizes the key parameters of these two types of organic scintillators.

**Table 1:** Key parameters of liquid and plastic scintillators

	plastic scint.	liquid scint.
1. Hydrogen / carbon ratio	$\approx 1.1$	$\approx 0, 1.2 - 2.0$
2. Scintillation efficiency	55 – 65 %	40 – 80 % anthracene
3. Scintillation spectrum $\lambda_{\max}$	370 – 490 nm	$\approx 425$ nm
4. Transparency	1 - 4 m	
5. Decay times	1.4 – 3 ns, 230 ns	2 – 4 ns
6. Pulse-shape discrimination	(yes)	yes
7. Doping for thermal sensitivity	yes	yes

The response of organic scintillators is determined by the energy distribution of the secondary particles, the non-linear light output functions, the influence of multiple scattering, wall effects and by the finite pulse-height resolution. At energies below 4.4 MeV, neutrons can only produce light charged particles in organic scintillation detectors by np scattering. In this energy range, the pulse-height distribution is determined by the rectangular energy distribution of recoil protons and their non-linear light output function. At higher energies also neutron-induced reactions with carbon nuclei contribute and modify the response, in particular at lower pulse height. Fig. 9 shows the cross sections of the reactions relevant for the response in the neutron energy range below 20 MeV and an example for the decomposition of total pulse-height response to monoenergetic neutrons according to the first interaction.

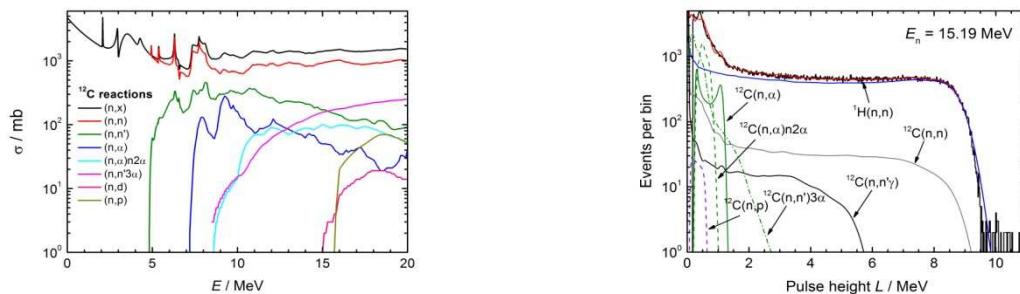


**Fig. 9:** The left panel shows the cross sections of the neutron induced relations relevant for modeling the response of scintillation detectors for neutron energies below 20 MeV. The experimental (histogram) and calculated (lines) differential pulse height response of a liquid scintillation detector to 15.19 MeV neutrons is shown on the right panel. The partial distributions are sorted according to the first interaction.

In this energy range the response of the detector can be modeled rather accurately, with the exception of small discrepancies caused by the insufficient description of the breakup

channels  $^{12}\text{C}(n,n'\alpha)$ . At higher energies, however, the discrepancies between the experimental and calculated pulse-height response are much larger.

Despite progress in the description of the response of scintillation detectors to neutrons, an experimental investigation of the response is still necessary, at least when small uncertainties are required, or for neutron energies above 20 MeV. The light output has to be determined experimentally, as it usually varies from detector to detector. The normalization of the response is most easily fixed by comparing calculated and measured pulse-height distributions in the pulse height region exclusively determined by np scattering, i.e. the ‘rectangular’ part of the response. White neutron beams are very suitable for this purpose, because the full pulse-height response can be determined as a function of neutron energy in a single experiment.

Liquid scintillation detectors can be built in very large volumes if the material is sufficiently transparent to its own scintillation light. This is very important, not so much for the detection of neutrons, but for the construction of large detectors for very rare events induced by neutrinos. For these detectors, technical and safety aspects are very important, such as availability, cost per volume, compatibility with container materials and, in particular, flammability and toxicity of the material. Very often these aspects rule out the classical trimethylbenzene-based liquid scintillators.

The strong quenching of the integral light yield for densely ionizing particles makes organic scintillation detectors difficult to use for low-energy neutrons. Here ‘doping’ of the scintillator with compounds containing isotopes with a large reaction cross section and a large positive  $Q$ -value, such as  $^{10}\text{B}$ ,  $^{155,157}\text{Gd}$ , or  $^6\text{Li}$  is an alternative. The high-energy secondary particles or photons resulting from neutron-induced reactions with the dopant produce sufficiently high signals even for thermal neutrons. In case of reactions emitting alpha particles, PSD techniques can be employed to improve the discrimination of events induced by neutrons and photons. Of course, ‘doping’ is most easily realized in liquid scintillators, but ‘doped’ plastic scintillators were developed as well. For liquid scintillators adverse effects of the dopant on the light yield and the PSD properties have to be minimized.

Inorganic scintillators such as  $^6\text{LiI}$  and in particular LiGlass scintillators remain very popular for detection of thermal neutrons. LiGlass scintillators consist of cerium-activated silicate glasses which contain up to 20 %  $\text{LiO}_2$ . The advantage of  $^6\text{LiGlas}$  scintillators is their stability and their large range of sizes. By using either  $^6\text{Li}$  or  $^7\text{Li}$  oxide, detectors with strongly different sensitivity to thermal neutrons can be produced. Since LiGlass has almost no PSD capability, discrimination of events induced by neutrons and photons is only possible by using a pulse-height threshold. A novel scintillator material for the detection of low-energy neutrons is cerium-activated  $\text{Cs}^6\text{LiYCl}_6$  (CLYC) [LEE12]. This material has a very large integral light yield, excellent PSD properties and a fast time response which facilitates efficient suppression of photon background and time-of-flight measurements. The crystals are, however, difficult to grow and not available in large sizes.

#### 2.2.2.4 Recoil telescopes

With sufficient effort put into the characterization of organic scintillation detectors, neutron fluence measurements with relative uncertainties in the order of 2 % can be performed. Nevertheless, proton recoil telescopes remain the best choice for neutron fluence reference instruments, because their response is determined exclusively by the differential np scattering cross section, the number of hydrogen atoms in the radiator material (usually polyethylene or tristearine) and the geometry of the instrument. Fig. 10 shows the schematic arrangement of the neutron source, the hydrogenous radiator and the aperture defining the solid angle for the detection of the recoil protons produced by np scattering in the radiator.

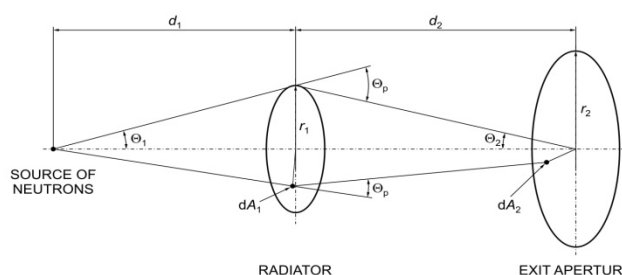


**Fig. 10:** Schematic layout of a recoil proton telescope. The radiator is a thin layer of homogeneous material, e.g. polyethylene. The solid angle for the detection of the recoil protons is defined by an aperture in front of the proton detector.

In most cases the detection efficiency is calculated semi-analytically. In the energy range below 20 MeV the classical Los Alamos design is often used. Here the radiator and the recoil proton detector are positioned in the neutron field. The aperture in front of the proton detector restricts the neutron scattering angles to a small range around an angle of  $180^\circ$  in the centre-of-mass frame. Since all part of the instruments are located in the neutron beam, the recoil protons have to be separated from neutron-induced background by requesting coincidences in additional transmission detectors arranged in front of the proton detector. Fig. 11 shows the recoil proton telescope T1 used as the fluence reference instrument for neutron energies between 1.2 MeV and 20 MeV at the PTB.

Due to the rather small detection efficiency, recoil telescopes must be positioned as close as possible to the neutron source. Hence, the precise measurement of this distance becomes crucial. At higher energies protons, deuterons, tritons and alpha particles are produced by  $^{12}\text{C}(n,x)$  reactions in the radiator in addition to recoil protons. They must be discriminated using  $\Delta E$ - $E$  particle identification. The contribution of protons from  $^{12}\text{C}(n,px)$  reactions can be determined separately by a measurement with a graphite radiator. Fig. 12 shows the separation of different particle species produced by 72 MeV neutrons in a polyethylene radiator. The telescope was mounted at an angle of  $20^\circ$  with respect to the collimated neutron beams to avoid excessive neutron-induced background.

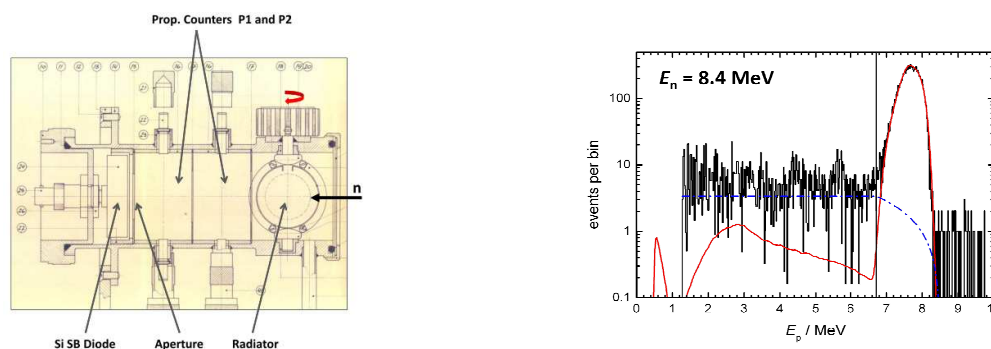


**Fig. 11:** The left panel shows the recoil proton telescope T1 of the PTB. The recoil protons emitted from the radiator pass two proportional counters and are registered in a surface barrier detector. The range of proton emission angles is defined by an aperture in front of the surface barrier detector. The right panel shows the measured (black histogram) and calculated (red solid line) energy distributions of the recoil protons. The dashed blue line indicates the extrapolation of the residual low-energy events under the recoil peak.

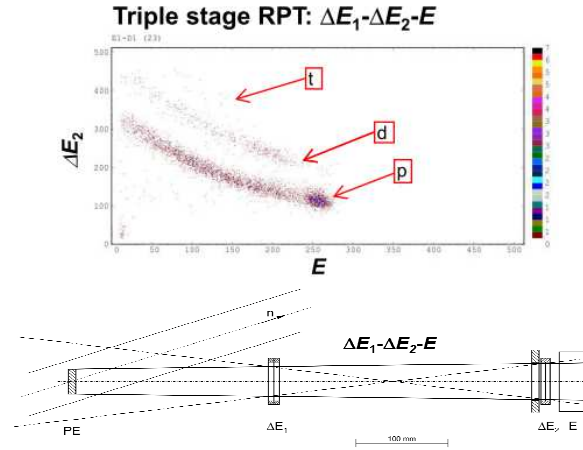


**Fig. 12:** Separation of the different hydrogen isotopes (upper panel) in a triple-stage  $\Delta E_1$ - $\Delta E_2$ - $E$  recoil proton telescope (lower panel). The quasi-monoenergetic neutron distribution with a peak neutron energy of 72 MeV was produced by the  $p+{}^7\text{Li}$  reaction. The  $\Delta E$  silicon PIN diodes had a thickness of 500  $\mu\text{m}$ . The  $E$  detector was a NaI scintillator. The telescope was positioned at an angle of  $20^\circ$  relative to the axis of the collimated neutron beam.

### 2.2.3 Fission ionization chambers

Fission ionization chambers are very useful secondary reference instruments for neutron measurements because of their simple and rugged construction and easy operation. The large positive  $Q$ -value of the fission process make these instrument almost immune against photon-induced ambient background. The fission process in  ${}^{235}\text{U}$  can be used for fluence measurements in the energy range from 100 keV up to 200 MeV. The large  ${}^{235}\text{U}(n,f)$  cross section at thermal energies and in the resonance region can cause problems when a background of low-energy neutrons is present. In such cases the neutron-induced fission process in  ${}^{238}\text{U}$  can be employed for neutron energies above 2.5 MeV. Because of rather small specific activity of  ${}^{235,238}\text{U}$ , the pile up of fission events and alpha particle background does not pose significant problems.

For neutron fluence measurements the details of the pulse height spectrum are irrelevant, as far as events induced by fission fragments can be clearly discriminated from events induced by alpha particles resulting from the radioactive decay of the fissile isotopes. Hence, the simple parallel-plate design shown in Fig. 13 can be employed for fluence reference instruments.

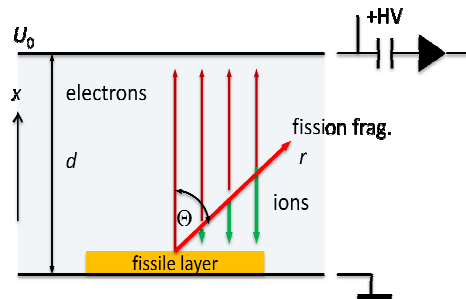


**Fig. 13:** Schematic design of a parallel-plate fission ionization chamber for neutron fluence measurements. The voltage is applied using the ‘forward biasing’ scheme, i.e. the secondary electrons drift to the opposite electrode.

The fission fragments are released in the fissile layers deposited on the cathode of the fission chamber. Secondary electron drifting in the electrical induce a voltage change  $\delta U$  on the anode which depends on the angle  $\Theta$  of the track relative to the normal on the cathode,

$$\delta U = \frac{e_0}{C} \int_0^T \left( \frac{1}{W} \frac{dE}{dr} \right) \cdot \left( 1 - \frac{r}{d} \cos \Theta \right) dr. \quad (4)$$

Here  $W$  and  $(dE/dr)$  denote the energy required to produce an ion pair and the differential energy loss of fission fragments in the counting gas, respectively. The capacity of the fission chamber is denoted by  $C$  and  $d$  is the distance between anode and cathode. The length of the fragment track in the counting gas is  $T = \min(R, d/\cos \Theta)$ , where  $R$  denotes the range of the fragment in the counting gas. For chambers operated at atmospheric pressure with P10 counting gas (90 % Ar, 10 % CH<sub>4</sub>), a distance  $d$  of about 5 mm is used which results in good separation between the signals induced by alpha particles and fission fragments, while keeping the total depth of the chamber small.

The neutron detection efficiency of fission ionization chambers is rather low, because the thickness of the fissile layer has to be restricted to less than 10 % of the range of the fission fragments, i.e. the mass per unit area is usually less than 500  $\mu\text{g}/\text{cm}^2$ . The neutron detection efficiency can be increased by using a stack of several fission chambers connected in parallel. The fission fragment detection efficiency  $\varepsilon_f$  of a fission ionization chamber is determined by the absorption of fragments in the fissile layers. It can be calculated analytically from the range  $R_f$  of fission fragments in the fissile material if a homogeneous layer can be assumed [CAR74],

$$\varepsilon_f = 1 - \frac{d}{2R_f} + \dots \approx 0.94 - 0.99. \quad (5)$$

Higher-order energy-dependent corrections arise from the anisotropy of the fragment emission and from incomplete transfer of momentum to the fission fragments. Depending on the thickness of the layer, the fission fragment detection efficiency ranges between 0.94 and 0.99. The relative energy dependence is less than  $\pm 0.5\%$ . As shown in Fig. 14, the homogeneity of the fissile layers influences the details of the pulse-height distributions, in particular the fraction of fission-induced events in the plateau region at small pulse height. Monte Carlo simulations indicate that for homogeneous layers a horizontal extrapolation can be used to determine the correction for those fission events lost in the region of the alpha-particle background.

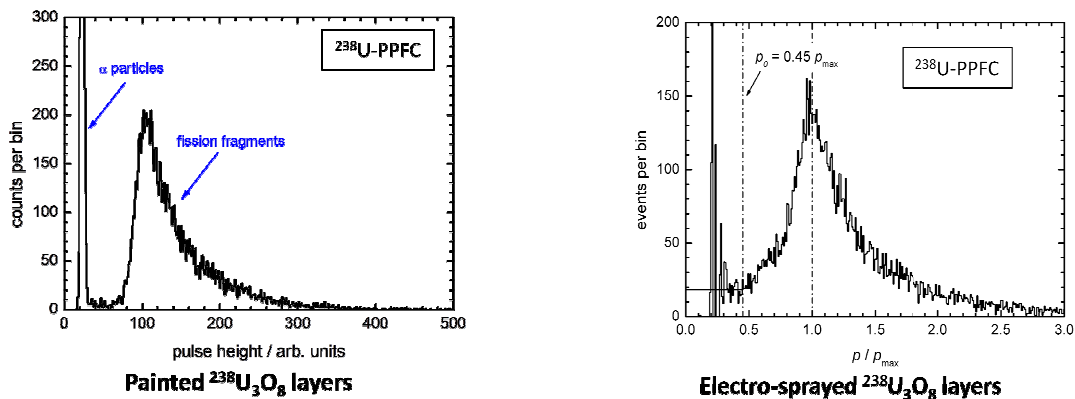


**Fig. 14:** Pulse-height distribution measured for a  $^{238}\text{U}$  fission ionization chambers with very homogeneous (left panel) and inhomogeneous (right panel) layers produced using different technologies. The chambers were operated in the ‘forward-biased’ mode. Horizontal extrapolations are used to determine the fission-induced events in the region of the alpha particle background.

The number of fissile atoms in the layers can be determined by weighing before and after deposition of the material on the electrode, if the chemical composition of the material is well defined and known. Alternatively, narrow-geometry alpha counting using solid state detectors

can be employed. For some isotopes, e.g.  $^{242}\text{Pu}$ , the half life for spontaneous fission is known so well that the product of the number of fissile atoms and the fragment detection efficiency can be determined from the measured rate of spontaneous fission events.

## 2.3 Techniques for neutron measurements

### 2.3.1 Time-of-flight measurements

The energy distribution of neutrons can be determined from a measurement of the flight time  $t$  required to travel a distance  $d$ . The flight time is most easily measured if the neutrons are generated in burst with durations of a few nanoseconds. Such neutrons beams or fields are produced by charged particle beams with a pulsed time structure incident on sufficiently thin neutron production targets. Detectors with time resolutions comparable to the duration of the neutron bursts at the position of the production target are used for measuring the time of arrival  $t_n$  at the detector relative to a reference signal derived from the charged particle beam pulses. The time delay of this reference signal to the ‘physical’ time of neutron production is constant, but usually unknown. Hence, the time of neutron production has to be determined from the time of arrival  $t_\gamma$  of the photons produced together with the neutrons and the velocity of light  $c$ ,

$$t = (t_n - t_\gamma) + d/c. \quad (6)$$

For neutron energies above a few MeV, relativistic kinematics has to be used to relate the neutron flight time  $t$  for a distance  $d$  to the neutron velocity  $v = d/t$  and energy  $E$ ,

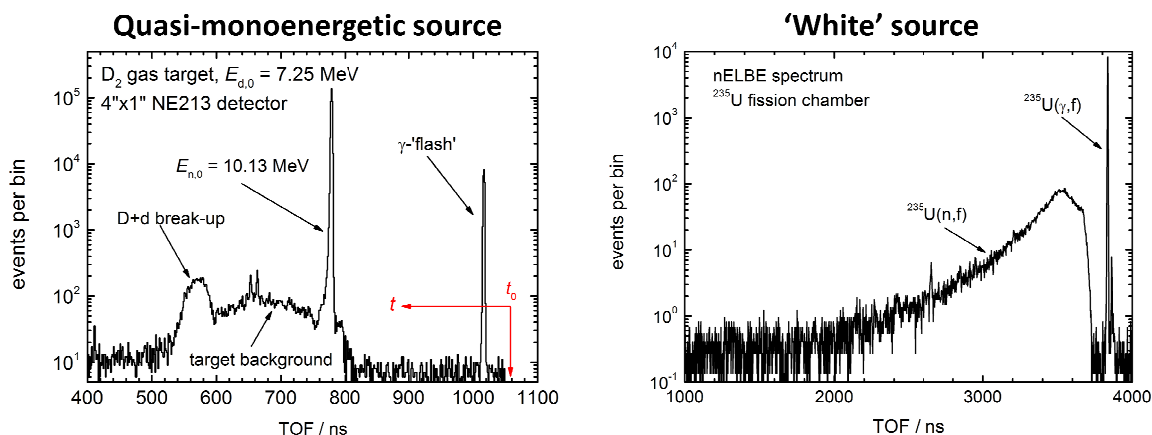
$$E = (\gamma - 1) \cdot mc^2, \quad \gamma = \frac{1}{\sqrt{1 - (v/c)^2}}. \quad (7)$$

Fig. 15 shows two typical time of flight distributions for a quasi-monoenergetic neutron source and a source with continuous (‘white’) energy distribution. It should be noted that eq. (7) assumes a point-like neutron production target and detector. Usually, however, the measured time difference between the detected arrival time of neutrons and photons includes also the transit times spent by the neutrons in the production target and the detector. Hence, corrections for these extra times have to be applied to eq. (7) which are usually expressed by an energy-dependent additional flight distance  $\delta d_{\text{eq}}(E)$ . The uncertainty  $\delta E$  of the neutron energy (energy resolution) achievable using this technique is limited by the uncertainty  $\delta t$  of the measured flight time and the uncertainty  $\delta d$  of the flight distance.

$$\frac{\delta E}{E} = (\gamma + 1)\gamma \frac{\delta v}{v}, \quad \frac{\delta v}{v} = \sqrt{\left(\frac{\delta t}{t}\right)^2 + \left(\frac{\delta d}{d}\right)^2} \quad (8)$$

The first component  $\delta t/t$  has contributions from the duration of the charged particle beam and the time resolution of the neutron detector, the second component  $\delta d/d$  has contributions from multiple scattering of the neutrons in the target and the detector, i.e. the distribution of flight distances  $d$ .

The effect of the size of the neutron detector on the time resolution is demonstrated in Fig. 16 which shows the time difference between the arrival of the neutrons on the surface of an organic scintillation detector and the time of the actual detection of the neutrons. The rectangular peak is due to the transit time through the detector while the exponential slope is caused by multiple scattering of the neutrons.



**Fig. 15:** Measured neutron time-of-flight distributions for a monoenergetic (left panel) and a ‘white’ (right panel). The indicated time  $\text{TOF} = t_{\text{start}} - t_{\text{stop}}$  is the time difference between the signal in detector ( $t_{\text{start}}$ ) and the reference signal ( $t_{\text{stop}}$ ) derived from the charged particle beam or the accelerator radiofrequency signal. The red symbol in the left panel show the location of the origin  $t_0$  for the physical flight time  $t$  in this ‘inverted’ TOF scale, as determined from the position of the peak corresponding to the  $\gamma$ -flash.

The time-of-flight technique can also be used to measure the energy distribution of secondary neutrons resulting from elastic or inelastic neutron scattering or (n,xn) reactions. In these cases the time-of-flight distributions are also broadened by the kinematical dependence of the neutron energy  $E$  of the emission angle  $\Theta$  because of the finite angular acceptance of the neutron detector. This is demonstrated in Fig. 17 for monoenergetic neutrons scattered off a polyethylene sample.

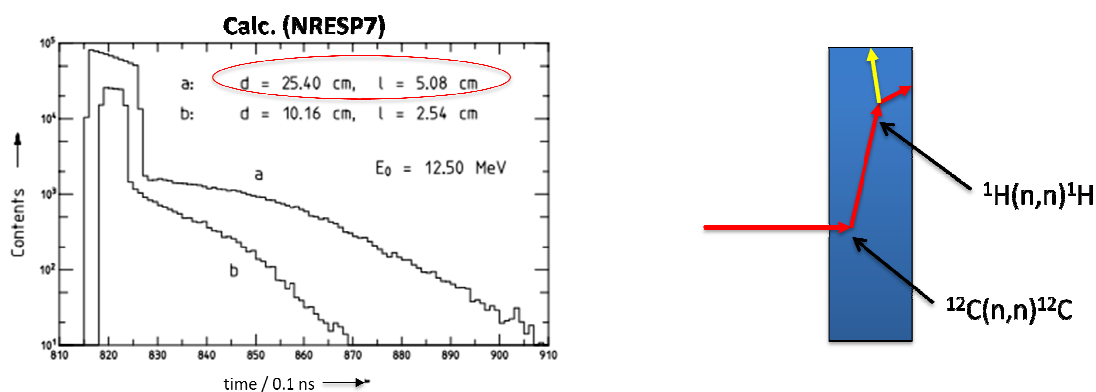


**Fig. 16:** Calculated distribution of neutron interaction times for cylindrical organic scintillation detector of with diameter  $d$  and height  $l$  for  $d \approx l$  and  $d \gg l$ .

As already mentioned above, organic scintillation detectors are the working horses for TOF spectrometry because of their fast time response of about 1 ns and their high neutron sensitivity due to the large np scattering cross section. The shape of scintillation detectors can be adapted to the needs of TOF measurements and photon-induced background can be discriminated using PSD techniques. Scintillation detectors are, however, difficult to apply for neutron energies below 1 MeV because of the quenching of the light production by low-energy recoil protons. Compared with scintillation detectors,  ${}^6\text{Li}$  Glas detectors show a slower time response of 3-4 ns and the strong resonance of the  ${}^6\text{Li}(n,t)$  cross section around 250 keV effects the time response. Other disadvantages are the strong sensitivity to thermal neutrons because of the  $1/v$  energy dependence of the  ${}^6\text{Li}(n,t)$  cross section and the large photon sensitivity of LiGlass detectors without significant PSD capability.

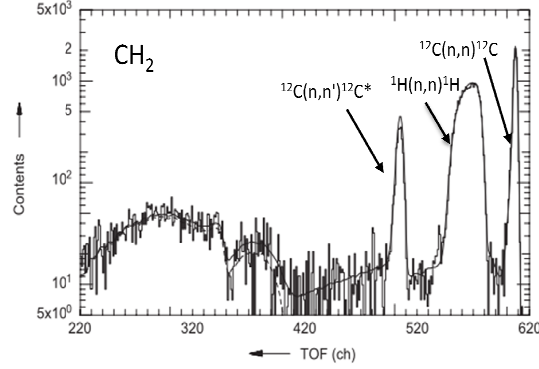


**Fig. 17:** Monoenergetic neutrons scattered off a polyethylene sample. The angular acceptance  $\delta\Theta$  of the scintillation detector was  $\pm 0.7^\circ$ . The strong kinematical broadening of the peak resulting from np scattering is due to the small target mass ( $A = 1$ ).

The TOF technique can even be applied for sources with a continuous time structure if a double scattering experiment is carried out, using an active radiator to ‘tag’ the neutrons. An example for such a ‘self-TOF’ device is the TOFOR spectrometer [GAT06] installed at the JET tokamak for the measurement of the neutron energy distributions produced during deuterium discharges. This device makes use of the fact that in an organic scintillation detectors only recoil protons produce a significant amount of scintillation light and carbon recoils are virtually ‘invisible’, i.e. only np scattering events are detected in an ‘active’ radiator consisting of a thin plastic scintillator. The energy  $E_{n'}$  of the scattered neutrons emitted at an angle  $\alpha$  is given by  $E_n \cos^2 \alpha$ . Hence, as shown in Fig. 18, neutron detectors arranged on a sphere of radius  $R$  together with the radiator will register the same time difference  $t$  to the signal from the active radiator and the energy  $E_n$  of the incident neutrons is given by

$$E_{n'} = E_n \cos^2(\alpha) \Rightarrow E_n = 2m \left( \frac{R}{t} \right)^2 \quad (9)$$

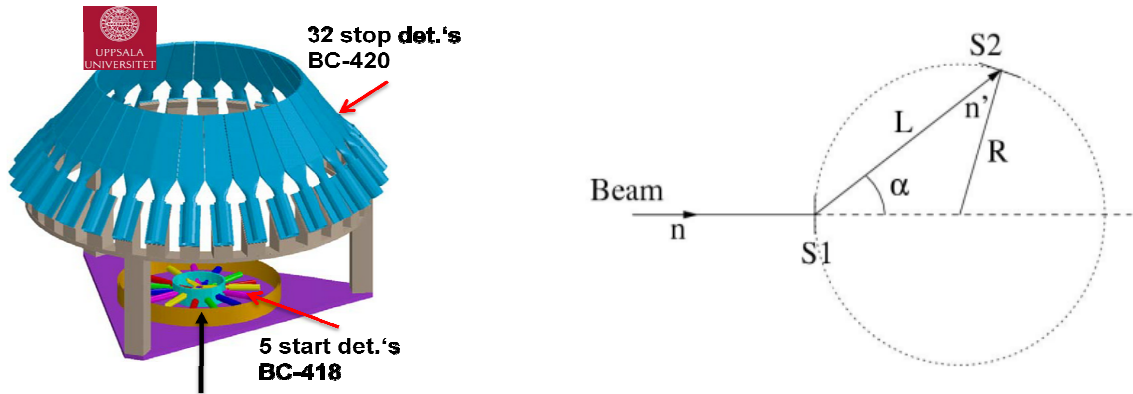


**Fig. 18:** Layout of the TOFOR spectrometer [GAT06] at the JET tokamak. The neutron detector and the active radiator are located on a sphere of constant TOF for the scattered neutrons. The spectrometer was designed to detect the 2.5 MeV neutrons from deuterium discharges.

Another important variant of the TOF technique is the slowing-down spectrometry. This technique uses the slowing down of high-energy neutrons in a large high- $Z$  moderator. The mean logarithmic energy loss per collision  $\xi = 2/(A+2/3)$  is very small. This results in a dependence of the mean neutron velocity  $v$  on the time  $t$  after production of the primary neutron with velocity  $v_0$  [BEC64],

$$v(t) = \frac{2}{\xi \Sigma_s t} \quad (v \ll v_0), \quad (10)$$

where  $\Sigma_s$  denotes the macroscopic scattering cross section of the moderator material. For a lead moderator ( $A = 208$ ), the spread of the slowing-down time and energy distributions are in the order of 5 % and 10 %, respectively. Hence, the semi-empirical relation

$$\bar{E}(t) = \frac{K}{(t-t_0)^2} \quad (11)$$

with the experimentally determined parameters  $K$  and  $t_0$  can be used to relate the time dependent count rate of a detector, e.g. a fission ionization chamber, exposed to a neutron field inside such a moderator to the mean energy  $\bar{E}(t)$  of the neutrons. The advantage of this spectrometer is that very high instantaneous neutron fluence rates can be produced which makes measurements with very small samples masses possible. Of course, the poor energy resolution of only 20 % to 30 % does not allow the resolution of resonances and other fine structures in the cross section. An example of such a spectrometer is the LANL lead slowing-down spectrometer [ROC05] which consists of a cube of 1.2 m<sup>3</sup> of very pure lead. The spectrometer is driven by an 800 MeV proton beam incident on a tantalum spallation target located at the center of the lead cube.

The most important restriction of ‘conventional’ time-of-flight spectrometry is the need to adapt the repetition frequency  $f$  of the beam to the chosen flight distance  $d$  to avoid ambiguities in the relation between the neutron energy  $E$  and measured flight time  $t$ . Neutrons below the frame-overlap threshold

$$E_o \approx \frac{1}{2} m(d f)^2 \quad (12)$$

have to be suppressed by a suitable pulse-height threshold or by filters to avoid neutrons produced by consecutive beam pulses to travel between source and detector at the same time. Hence, a good energy resolution using a large flight distance can only be achieved at a reduced repetition frequency which is often difficult to achieve, in particular for sources driven by cyclotrons, and compromises the mean source emission rate in most cases.

## 2.3.2 Neutron spectrometry

### 2.3.2.1 General aspects

Time-of-flight spectrometry is the method of choice for measurements of neutron energy distributions but there are many situations where this technique is not applicable, for example for quasi-stationary sources, large distributions of possible flight paths, e.g. in shielding benchmarks, or for environmental measurements where neutron energies from a few meV to several hundred MeV are relevant. Such measurement problems can be solved using detectors for which the so-called response function  $R(L, E)$ , i.e. the relation between the detector signal  $L$  and the neutron energy  $E$ , is well known. The distribution  $(dN/dL)$  of detector signals is given by

$$(dN/dL) = \int R(L, E) \cdot \Phi_E dE \rightarrow N_i \approx \sum_j R_{i,j} \Phi_j \quad (13)$$

Eq. (13) is a Fredholm integral equation of the first kind. It can be approximated by a matrix equation relating the fluence  $\Phi_j$  in the energy bin  $j$  to the number of events  $N_i$  in detector signal bin  $i$ . Techniques for the ‘solution’ of this equation are called ‘unfolding’ methods and the measurement of neutron energy distributions using these techniques is usually termed ‘neutron spectrometry’. Fig. 19 illustrates the problem of getting from the space of data  $N_i$  to the space of possible solutions  $\Phi_j$ .

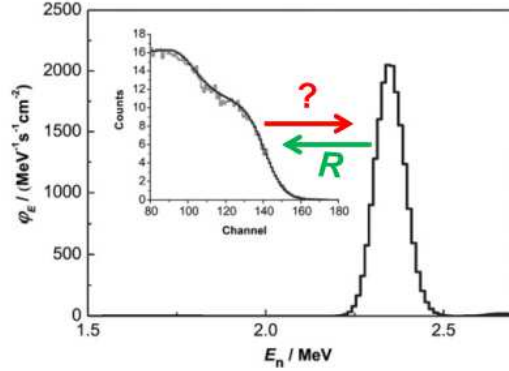


**Fig. 19:** Relation between the spectral fluence distribution  $\Phi_E$  and the distribution of detector signals  $L$  (insert). The inference of the neutron energy distribution from the distribution of signals using the detector response matrix  $\mathbf{R}$  and all available preinformation is termed ‘neutron spectrometry’.

Formally, the matrix equation (13) can be solved by direct inversion,

$$N \approx \mathbf{R} \cdot \Phi \Rightarrow \Phi \approx (\mathbf{R}^T \cdot \mathbf{R})^{-1} \cdot \mathbf{R}^T \cdot N, \quad (14)$$

but the matrix  $(\mathbf{R}^T \cdot \mathbf{R})^{-1}$  is usually ill-conditioned, if it exists at all. The straight-forward direct inversion will usually effect an increase in the ‘noise’ of the resulting fluence distribution and eventually even lead to negative fluence values  $\Phi_j$ . Moreover, eq. (13) does not account for the uncertainties  $u_i$  of the measured number of events in detector signal bin  $i$ . A more realistic version of eq. (13) would be

$$N_i + u_i = \sum_j R_{i,j} \Phi_j \quad (15)$$

which still neglects the uncertainty of the response matrix  $\mathbf{R}$ .

Usually there is a multitude of solutions  $\Phi_j$  which would produce the same distribution of detector signal  $N_i$  via eq. (15). Hence, it is not requested to find the ‘exact’ solution which might not exist at all. Instead, an approximate solution is sought which is consistent with the experimental data and all available preinformation on the spectral fluence distribution.

Iterative methods to ‘solve’ the unfolding problem starting from a ‘guess solution’ were developed already decades ago, but their mathematical foundation is sometimes not entirely clear. The least squares methods use a linearised approximation to eq. (15) and are capable of including the correlated uncertainties of the data and the response matrix. Regularization methods address the problem of the amplification of ‘noise’, i.e. the ‘unphysical’ fluctuations in the solutions, by adding constraints to enforce numerical stability and smoothness of the solution. There are also stochastic techniques, e.g. Monte Carlo methods or genetic algorithms, for solving the unfolding problem.

The most advanced methods make explicit use of Bayes equation and understand the solution of the unfolding problem as a process of learning which uses the measured distribution of signals and the information on the detector response to add more information to the already available pre-information on the neutron spectrum. Examples are methods based on the maximum entropy principle or the method of Bayesian parameter estimation starting from an analytical model of the neutron energy distribution. A short overview of these techniques is given in [REG10].

From the experimental side, neutron spectrometry can either aim at resolving details of the neutron energy distribution at the expense of covering many decades of neutron energy, or can try to determine the neutron distribution over a large logarithmic energy intervall with a resolution of only a few ten bins per decade of neutron energy.

### 2.3.2.2 High-resolution spectrometry

High-resolution spectrometry requires detectors with a strong dependence of the response on neutron energy, but the response matrix does not need to be ‘diagonal’. Typical examples are measurements of the neutron energy distributions produced in plasma discharges. These measurements are carried out using organic scintillation detectors. The location of the recoil edge in these detectors is related to the neutron energy by the integral light yield and the response matrix is almost trigonal. It can be calculated using Monte Carlo simulation codes or determined experimentally using monoenergetic neutrons. The broadening of the recoil edge (pulse height resolution) determines the energy resolution of the neutron distribution inferred from the pulse-height distributions. With response matrices of high quality a neutron energy resolution of about 1/5 of the pulse-height resolution can be achieved. Fig. 20 shows two examples of neutron distributions obtained for JET discharges with pure ohmic and ohmic plus neutral beam heating [ZIM06].

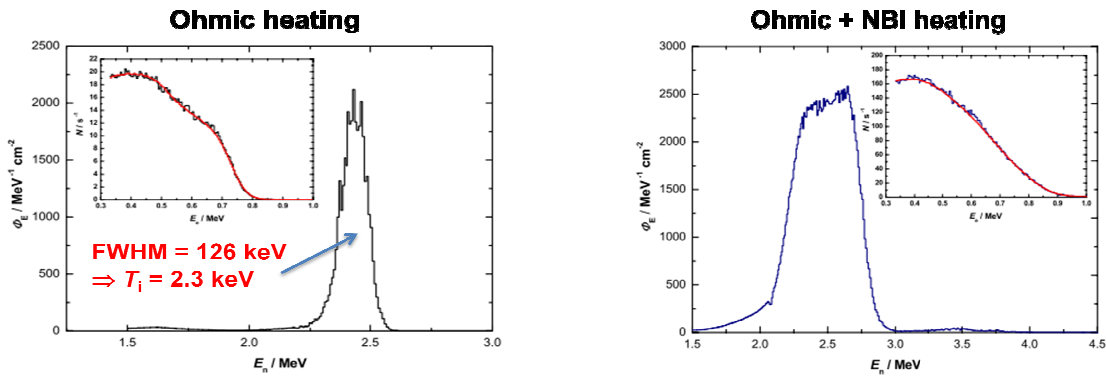


**Fig. 20:** Neutron energy distributions produced determined from pulse-height distributions measured using a cylindrical BC501A scintillation detector (2" in diameter and length) [ZIM06]. The neutrons were produced during deuterium discharges with ohmic and neutral beam heating at the JET tokamak.

The biggest danger of unfolding methods is the occurrence of so-called artifacts which result from imperfections in the response matrices, in particular if larger energy intervals are to be covered. This is demonstrated in Fig. 21 which show neutron distributions produced with a 643 keV deuteron beam incident on a 1 mg/cm<sup>2</sup> Ti(T) target containing about 1 % deuterium as an impurity. The distributions exhibits two distinct peaks from the D(d,n)<sup>3</sup>He and the T(d,n)<sup>4</sup>He reactions at about 3 MeV and 15.5 MeV, respectively. The neutron energy distribution obtained using an experimentally determined response function shows an additional structure between 10 MeV and 12 MeV which is caused by imperfections of this particular response function.

The difficulties incurred with unfolding procedures can be reduced if the response matrix of the detector can be made as ‘diagonal’ as possible. For recoil detectors this can be achieved using reactions with two charged particles in the exit channel, such as the <sup>3</sup>He(n,p)T reactions. Then the maximum energy  $E_{\text{dep}}$  deposited in the detector is given by

$$E_{\text{dep}} = E_n + Q. \quad (16)$$

and a maximum related to to these events with full energy deposition by the two secondary particles is expected in the response. In addition to these peaks events without full energy deposition or parasitic events from competing reactions might causes a low-energy continuum in the response. For example, in a <sup>3</sup>He proportional counter the off-diagonal contributions to the response functions are mainly due to edge effects and elastic scattering on <sup>3</sup>He, i.e. <sup>3</sup>He recoils. The same technique is applied in a <sup>3</sup>He or a <sup>6</sup>Li sandwich spectrometer in which the two charged secondary particles emitted from a small <sup>3</sup>He gas volume or thin <sup>6</sup>Li radiator in are detected in two opposite silicon solid state detectors.

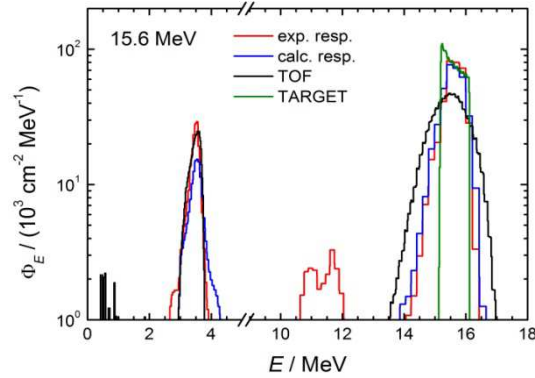


**Fig. 21:** Neutron energy distributions obtained for a 643 keV deuteron beam incident on a 1 mg/cm<sup>2</sup> Ti(T) target with a 1 % deuterium impurity. The blue and red histograms were unfolded using a calculated and a experimentally determined response matrix. The black histogram was obtained using the time-of-flight technique. The green histogram shows the spectral distribution calculated for the nominal target properties without the deuterium impurity present. The stronger broadening of distribution obtained using the time-of-flight technique is due to the large duration of the low-energy deuteron bunches.

In recoil telescope the angular range of recoil protons is confined to a small range of proton emission angles close to 0° which result in a peaked response compared with a scintillation detector. Hence, the pulse-height distributions of recoil telescopes can be unfolded to obtain the neutron energy distribution. In modern designs, additional detectors with spatial resolution are used to track individual recoil protons and to use the information on the emission angle to improve the unfolding. The disadvantage of this technique is the rather high low-energy cutoff imposed by the energy loss in the radiator and the tracking detectors.

Another technique to obtain a diagonal response matrix with a scintillation detector is the so-called ‘capture-gated’ spectrometry. This technique uses scintillation detectors which are doped with an isotope with a high cross section for thermal neutrons, e.g. <sup>155,157</sup>Gd, <sup>6</sup>Li or <sup>10</sup>B. Events with complete energy deposition by multiple np scattering are selected by requesting a coincidence of the prompt scintillation signal from recoil protons with delayed signal from the reaction of the thermalised neutrons with the dopant. Compared with normal scintillation detectors, a peaked pulse-height response is obtained for neutron energies up to 10 MeV.

### 2.3.2.3 Low-resolution spectrometry

The classical way to perform low-resolution spectrometry is to determine neutron energy distributions using activation foils. In the fast neutron energy range, endothermic reactions with radioactive product nuclei can be used to cover a given energy range. Ideally, reactions are selected which show steeply rising cross sections  $\sigma_i$  ( $i = 1 - n$ ) above the threshold energies  $E_{th,i}$  with  $E_{th,i} < E_{th,i+1}$  and a decrease at higher energies. Hence, each reaction is particularly sensitive to a certain energy range and the neutron fluence  $\Phi_j$  ( $j = 1 - m$ ) in the energy bin  $j$  can be determined from the measured production rate  $P_i$ , in an activation foil with  $N_i$  target nuclei,

$$P_i = N_i \sum_j \int_{E_j}^{E_{j+1}} \sigma_i \Phi_{E,j} dE \approx N_i \sum_j \bar{\sigma}_{i,j} \Phi_j. \quad (17)$$

using an unfolding procedure. Here  $\Phi_{E,j}$  and  $\bar{\sigma}_{i,j}$  denote the spectral fluence distribution in energy bin  $j$  and the spectrum-averaged cross section in this bin, respectively. For neutron

energy distributions containing slow and thermal neutrons, exothermic capture and fission reaction have to be used in addition to cover the full energy range.

The same technique is applied with active detectors in the so-called Bonner sphere spectrometers (BSS). A BSS consists of a set of spherical  $^3\text{He}$  proportional counters embedded in polyethylene moderators of different diameters. As shown in Fig. 22, this results in a fluence response  $R_\Phi(E) = N/\Phi$  which varies slowly as function of neutron energy and peaks at an energy which is characteristic for the size of the moderator. At high energies, pure polyethylene moderators would become too inefficient. Therefore, combinations of polyethylene with lead or copper shells are used to decrease the mean neutron energy efficiently by inelastic scattering and multiply the incident neutrons by (n,xn) reactions.

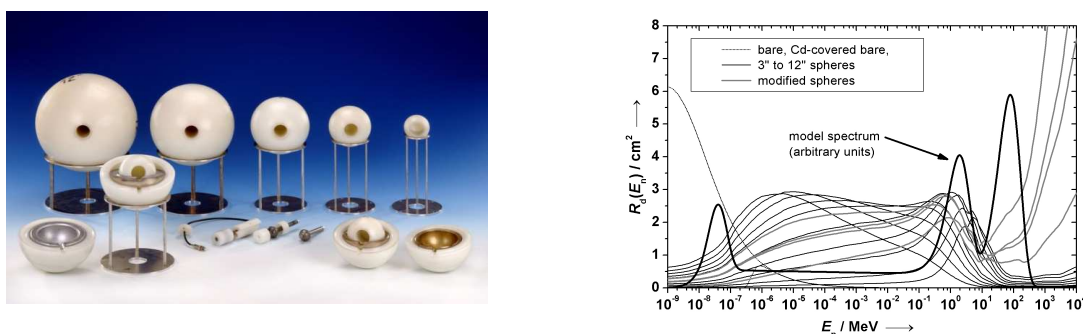


**Fig. 22:** The Bonner sphere spectrometer of the PTB (left panel) and its fluence response (right panel). The spectrometer consists of several spherical  $^3\text{He}$  proportional counters embedded in polyethylene moderators. Bare counters and moderators with copper or lead shell are used to enhance the sensitivity to thermal and high-energy neutrons, respectively. The thick solid line in right panel shows a typical energy-weighted spectral fluence distribution ( $E \cdot \Phi_E$ ) of a partially moderated source of fast or high-energy neutrons.

Low-resolution spectrometry is usually employed to characterize neutron fields encountered inside or behind shieldings or in moderated multiplying assemblies. These neutron energy distributions are usually quite similar and differ mainly in the relative magnitude of their prominent spectral features: the thermal peak, the slowing-down continuum, the evaporation peak and the high-energy ‘spallation’ peak. These structures can be described by simple analytical models, involving only a limited number of parameters. Hence, Bayesian parameter estimation can be employed to determine values of these parameters and their covariance matrix from the measured event rates of the Bonner sphere detectors.

### 2.3.3 Spatial neutron distributions

The spatial distribution of the neutron fluence is often required to evaluate the expected count rate in collimated neutron beams with a radially varying intensity profile. The most simple solution is to use an  $\text{BaFBr:Eu}^{2+}$  image plate with a suitable converter to produce charged particles. This phosphor has a large dynamic range with linear response, allows spatial resolutions in the order of 0.1 mm to be achieved and can be easily re-used after erasure with visible light. In the fast energy range, polyethylene sheets can be used as converter; in the slow energy range radiative capture in the  $^{151,153}\text{Eu}$  activator atoms can be employed. An image produced without converter can be used to subtract background effected by thermalized neutrons and by photons. Fig. 23 shows the intensity distribution in an high energy neutron beam recorded with an image plate. The biggest disadvantage of image plates is the lacking capability to discriminate the neutron energy. This can be circumvented to some extent by using the image plate to produce an autoradiograph of activation foils with different reaction thresholds.

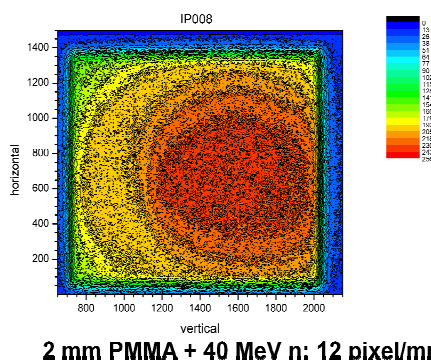


**Fig. 23:** Intensity distribution of a quasi-monoenergetic 40 MeV neutron beam obtained using a BaFBr:Eu<sup>2+</sup> image plate with a 2 mm lucite converter.

The spatial fluence distributions in collimated neutron beams with broad energy distributions are usually energy dependent. Therefore, active detectors with spatial resolution are required to provide images for different neutron energy windows. These windows are defined using the time-of-flight technique. The micromegas detectors [PAN04] uses a combination of solid-state <sup>6</sup>Li or <sup>10</sup>B converters and a gaseous conversion gap (He+isobutane, Ar+isobutane counting gases, gap width 3 mm) to convert neutrons to charged particles. The primary ionisation is amplified in an amplification gap separated from the conversion gap by a micromesh structure. Several strips and pad structures are used to provide one and two dimensional images. Fig. 24 shows the layout of this detectors and a series of beam profiles measured at the n\_TOF neutron beam facility [BEL13]. Spatial resolutions of about 0.5 mm were achieved using this detector.

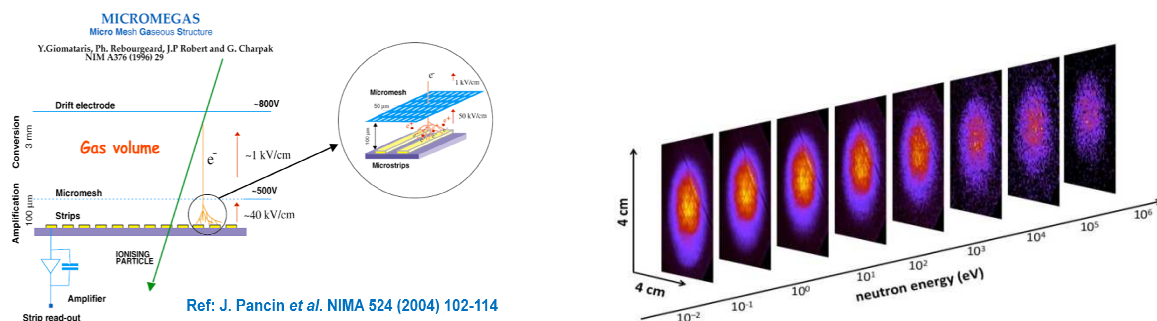


**Fig. 24:** Layout of the Micromegas detector (left panel) [PAN04] and beam profile of the n\_TOF neutron beam (right panel) [BEL13].

### 3 Absolute methods, quality assurance

#### 3.1 Associated particle methods

Neutron measurements are usually carried out relative to reference cross sections. Moreover, the detection efficiency of the reference instruments depends also on the knowledge of properties of ‘artifacts’ such the hydrogen content of radiators or the mass of fissile layers. The only technique which can at least in principle be used to measure the neutron fluence by pure counting is the so-called associated particle (AP) technique. This method uses the strict correlation of neutrons and charged particles in neutron-producing two-particle reactions, such as  $D(d,n)^3\text{He}$ ,  $T(p,n)^3\text{He}$  or  $T(d,n)^4\text{He}$ . In these reaction the number  $Y_n(\Theta_n)$  of neutrons emitted per unit solid angle at an emission angle  $\Theta_n$  in the laboratory

frame, the so-called yield, is related to the number  $Y_{cp}(\Theta_{cp})$  of charged secondary particles per unit solid angle at the kinematically correlated angle  $\Theta_{cp}$ ,

$$Y_n(\Theta_n) = \left( \frac{d \cos(\Theta_{cp})}{d \cos(\Theta_n)} \right) (E_{proj}) \cdot Y_{cp}(\Theta_{cp}). \quad (18)$$

For a given reaction and neutron emission angle  $\Theta_n$ , the quantity relating the two yields depends only on the projectile energy  $E_{proj}$ . For sufficiently thin neutron production targets this energy is well-defined. Hence, the neutron fluence  $\Phi = Y_n/d^2$  at a distance  $d$  from the target can be determined from the measurement of the yield  $Y_{cp}$  of associated charged particles using a solid state detector with a detection efficiency very close to one. Fig. 25 shows a typical AP setup for the  $T(d,n)^4He$  reaction.

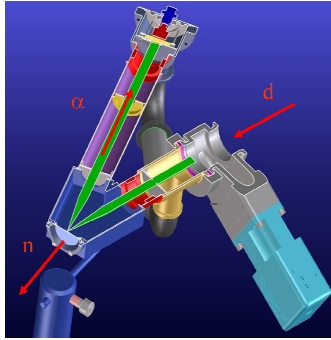


**Fig. 25:** AP setup for the  $T(d,n)^4He$  reaction. The associated alpha particles are detected at an emission angle  $\Theta_{cp}$  of  $150^\circ$  using a solid state detector. The effective solid angle covered by this detector is defined by an aperture located directly in front of the detector. The emission angle of the associated neutrons depends on the projectile energy  $E_{proj}$ . For 110 keV deuterons, the emission angle  $\Theta_n$  of the associated neutrons would be  $26.5^\circ$ .

The AP method is conceptually very appealing, but in real experiments corrections have to be applied for the effects of neutron transport in the scattering chamber and for the ion transport in the target, in particular for multiple scattering. For low projectile energies also the dependence of the kinematical factor in eq. (18) on the projectile energy cannot be neglected.

The kinematical factor is not needed if the correlations between individual events in the neutron and the charged particle detector are used, i.e. the neutrons are individually ‘tagged’ by detecting the associated charge particle. Using the time correlated associated particle method (TCAP) the detection efficiency  $\varepsilon$  of a neutron detector positioned at the angle  $\Theta_n$  is given by

$$\varepsilon = \frac{N_{n,cp}}{N_{cp}} \quad (19)$$

where  $N_{n,cp}$  denotes the number of detected coincident neutron and charged-particle events and  $N_{cp}$  is the total number of charged-particle events. Eq. (19) assumes that the cone of associated neutrons defined by the charged-particle detector is completely intercepted by neutron detector, including the broadening induced by the straggling of the charged particle in the target. In reality corrections for neutrons missing the neutron detector have to be applied. The total uncertainty achieved using the AP or TCAP methods range between 2 % to 3 %.

Associated particle methods can also be used with isotopes undergoing spontaneous fission, e.g.  $^{242}Cf$ . Here the fission neutrons are tagged by detecting the associated fission fragments in a small ionization chamber. Since the emission of neutrons from the fission fragment is a statistical process, the mean number  $\bar{\nu}$  of neutrons per fission has to be known with sufficiently small uncertainty for. The energy distribution of the neutrons can be

determined using the time-of-flight technique because small-size fission chambers allow time resolutions of about 1 ns to be achieved.

### 3.2 International key comparisons

Several neutron metrology institutes (NMIs) worldwide provide calibration capabilities for neutron detectors in the fast energy range. The neutron reference fields are produced and characterized according to the relevant ISO standards which describe monoenergetic neutron reference fields with mean energies of 24 keV, 144 keV, 250 keV, 565 keV, 1.2 MeV, 2.5 MeV, 5 MeV and 14.8 MeV. At most of the NMIs, however, the energy range up to 20 MeV can be covered. Depending on the accelerator infrastructure, neutron fields with intermediate energies can be produced as well, with exception of the so-called gap region between 7 MeV and 14 MeV where no reaction producing only monoenergetic neutrons is available. At the PTB neutron beam facility a CV28 cyclotron is used to cover the gap region with quasi-monoenergetic neutron reference fields produced with the  $D(d,n)^3\text{He}$  reaction and deuteron beams with energies up to 13.5 MeV.

The ultimate proof of the quality of the calibration services offered by the NMIs are the regular key comparisons organized by the Bureau International des Poids et Mesures (BIPM). In these exercises, all participants have to measure the yield  $Y$  per unit count of a very stable monitor in several neutron fields at one selected neutron beam facility. Fig. 26 shows the results of the most recent comparison carried out at four neutron energies [GRE14]. The uncertainties of the key comparison reference values (KCRV), i.e. the mean value of all results obtained by the participants, usually ranges around 1 % to 1.5 % and the standard deviation of the results between 2 % and 4 %.

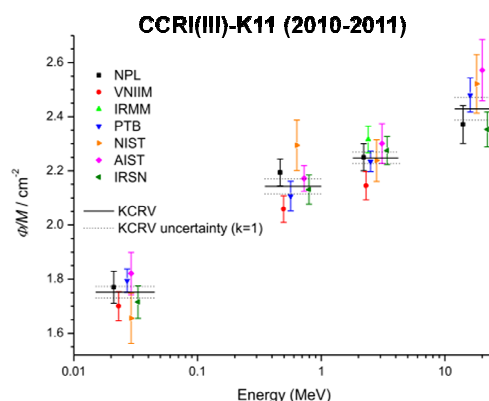


**Fig. 26:** Results of the most recent BIPM key comparison CCRI(III)-K11 of fast neutron fluence measurements [GRE14]. All participants had to determine the fluence per unit monitor count at 1 m distance from the target, corrected for attenuation in air. The measurements were carried out the AMANDE neutron beam facility of the Institut de Radioprotection et Surete Nuclaire (IRSN) in Cadarache/France.

### References

- [ARN91] R. Arndt, *Nucleon-nucleon Elastic Scattering Analysis at VPI&SU*, Proc. of a specialists meeting on neutron cross section standards for the energy region above 20 MeV, Uppsala, Sweden, 21st-23rd May 1991, Organisation for Economic Co-Operation and Development, report NEANDC-205'U'
- [BEC64] K.H. Beckurts, K. Wirtz, *Neutron Physics*, Springer Verlag, Berlin 1964
- [BEL13] F. Belloni, F. Gunsing and T. Papaevangelou, *Micromegas for Neutron Detection and Imaging*, Mod. Phys. Letters A **28** (2013) 1340023

- [BRO79] F.D. Brooks, *Development of organic scintillators*, Nucl. Instr. and Meth. **162** (1979) 477-505
- [CAR74] G.W. Carlson, *The Effect of Fragment Anisotropy on Fission-Chamber Efficiency*, Nucl. Instr. and Meth. **119** (1974) 97-100
- [CHA32] J. Chadwick, *Possible Existence of a Neutron*, Nature **129** (1932) 312
- [GAT06] M. Gatu Johnson et al., *The TOFOR Spectrometer and its First Use at JET*, Rev. Sci. Instrum. **77** (2006) 10E702
- [GOM10] M.B. Gómez Hornillos et al., *First Measurements with the BEta deLayEd Neutron Detectors (BELEN-20) at JYFLTRAP*, J.Phys. Conf. Series **312** (2010) 052008
- [GRE14] V. Gressier et al., *International Key Comparison of Neutron Fluence Measurements in Monoenergetic Neutron Fields – CCRI(III)-K11*, Metrologia **51** (2014) Techn. Suppl. Series 06009
- [HAN47] A.O. Hanson and J.L. McKibben, *A neutron detector having uniform sensitivity from 10 keV to 3 MeV*, Phys. Rev. **72** (1947) 673-677
- [KNO10] G.F. Knoll, *Radiation Detection and Measurement*, 4<sup>th</sup> Edition, John Wiley & Sons, New York 2010
- [LEE12] D.W.Lee et al., *Pulse-Shape Analysis of Cs<sub>2</sub>LiYCl<sub>6</sub>:Ce Scintillation for Neutron and Gamma-Ray Discrimination*, Nucl. Instr. and Methods in Phys. Res. A **664** (2012) 1-5
- [LEO09] W.R. Leo, *Techniques for Nuclear and Particle Physics Experiments*, 2<sup>nd</sup> edition, Springer Verlag, Berlin 2009
- [MAR60] J.B. Marion, J.L. Fowler, *Fast neutron physics, part I and part II*, Interscience Publishers, Inc., New York 1960
- [PAN04] W. Pancin et al., *Measurement of the n\_TOF Beam Profile with a Mocomegas Detector*, Nucl. Instr. and Methods in Phys. Res. **524** (2004) 102-114
- [POE73] W.P. Poenitz, *The Black Neutron Detector*, Nucl. Instr. and Methods **109** (1973) 413-420
- [REG10] M. Reginatto, *Overview of Spectral Unfolding Techniques and Uncertainty Estimation*, Radiat. Measurements **45** (2010) 1323-1329
- [ROB04] N.J. Roberts, H. Tagziria and D.J. Thomas, *Determination of the Effective Centres of the NPL Long Counters*, NPL Report DQL RN004, National Physical Laboratory, Teddington 2004
- [ROC05] D. Rochman et al., *Characteristics of the Lead Slowing-Down Spectrometer coupled to the LANSCE Accelerator*, Nucl. Instr and Methods in Phys. Res. A **550** (2005) 397-413
- [THO11] D.J. Thomas, R. Nolte, V. Gressier, *Neutron Metrology*, Metrologia **48** (2011), and following articles in this volume
- [ZAI12] N. Zaitseva et al., *Plastic Scintillators with Efficient Neutron/Gamma Pulse Shape Discrimination*, Nucl. Instr. and Methods in Phys. Res. A **668** (2012) 88-93
- [ZIM06] A. Zimbal et al., *High Resolution Neutron Spectrometry with Liquid Scintillation Detectors for Fusion Applications*, Proceedings of the International Workshop on Neutron Detectors and Applications, Cape Town, April, 3-6, 2006, Proc. Science **PoS(FNDA2006)** 035, available online at <http://pos.sissa.it>